https://doi.org/10.5194/egusphere-2024-4019
Preprint. Discussion started: 10 January 2025

JLH Mark2 - An Improved Opto-Mechanical Approach to Open-Path *in situ* Water Vapor Measurement in the Upper Troposphere / Lower Stratosphere

Robert L. Herman[1], Robert F. Troy[2,3], Kim M. Aaron[1], Isabelle Sanders[1], Kevin Schwarm[1], J. Eric Klobas[4], Aaron Swanson[4], Andrew Carpenter[4], Scott Ozog[4], Keith Chin[3], Lance E. Christensen[1], Dejian Fu[1], Robert A. Stachnik[3], Ram Vasudev[3]

[1]Jet Propulsion Laboratory, California Institute of Technology, 4800 Oak Grove Drive, Pasadena, California, 91109, USA.
[2]Robert Troy Engineering, Los Angeles, California.
[3]Formerly at Jet Propulsion Laboratory.
[4]Northrup Grumman Corporation.

Correspondence to: Robert L. Herman (Robert.L.Herman@jpl.nasa.gov)

Abstract. To improve the accuracy and precision of in situ water vapor measurements from aircraft, a new opto-mechanical design was implemented on the JPL Laser Hygrometer Mark2. The first JPL Laser Hygrometer (JLH Mark1), originally developed in mid-1990s, provided airborne in-situ water vapor measurements for 15 years from several platforms, including the NASA ER-2 and WB-57 aircraft. Due to heavy use over the years and aging of the instrument parts, many of the components in JLH Mark1 have been modified and replaced. This instrument paper reports the redesigned opto-mechanical structure of the instrument, new data retrieval algorithms, and updated data analysis procedures. These improvements are described in this paper, along with recent laboratory and field performance, and a comparison with other water vapor instruments. Key changes in the redesigned instrument have significantly improved the performance, as demonstrated during the NASA Studies of Emissions and Atmospheric Composition, Clouds and Climate Coupling by Regional Surveys (SEAC^{4}RS) field mission and eight years of subsequent science flights on the Northrup Grumman Corporation Flying Test Bed (FTB).

1 Introduction

Atmospheric measurements of water vapor in the upper troposphere and lower stratosphere (UTLS) are important for better understanding Earth's climate because UTLS water has a significant impact on climate despite its low concentrations. Through the radiative impact of water vapor (Solomon et al., 2010) and cirrus clouds, climate is strongly affected by atmospheric water. Clouds continue to be one of the biggest sources of uncertainty in climate prediction (Boucher et al., 2013, Davis et al., 2007). An addition climate contribution from clouds is due to aircraft. In the upper troposphere, a significant fraction of the area are ice super saturated regions (e.g., Troy, 2007; Gettelman et al., 2006; Heymsfield et al., 1998). In such an environment, aircraft engine combustion products water vapor and soot lead to ice nucleation, persistent contrails and aircraft induced cirrus clouds. Burkhardt and Kärcher (2011) found that aircraft induced cirrus are the largest net (warming) effective radiative forcing term from aviation, larger even than the radiative forcing term from CO_2 emissions from aircraft (Lee et al., 2021). There is a renewed interest in minimizing contrails in commercial aviation, which has led to the aircraft campaign coordinated by the Northrop Grumman Corporation and described herein.

https://doi.org/10.5194/egusphere-2024-4019
Preprint. Discussion started: 10 January 2025

The JPL Laser Hygrometer (JLH) for *in situ* UT/LS water vapor measurements has been developed and tested over many years. The initial version JLH Mark1(a) instrument provided airborne measurements from the NASA ER-2 aircraft (May, 1998). Several years later, a similar JLH Mark1(b) was developed by R. D. May at JPL for the NASA WB-57F aircraft. Both instruments are open-path near-infrared tunable diode laser absorption spectrometers designed to accurately measure atmospheric water vapor concentration from aircraft. The two JLH Mark1 instruments were among the first laser hygrometers developed for airborne measurements and had a fifteen year history of aircraft flights in NASA UT/LS field missions (see Table 1) for scientific studies of atmospheric water vapor, clouds and UT/LS transport (e.g., Hintsa et al., 1999; Hurst et al., 1999; Kley et al., 2000; Gates et al., 2002; Danilin et al., 2003; Herman et al, 2003; Lee et al., 2004; Hallar et al., 2003; Ray et al., 2004; Ridley et al., 2004; Gao et al., 2004; Jensen et al., 2005; Garrett et al., 2005; Gao et al., 2006; Richard et al., 2006; Gensch et al., 2008; and Froyd et al., 2010).

Due to heavy use over the years and aging of the instrument parts, many of the components in JLH Mark1 have been modified and replaced. For example, extensive exposure to rocket plumes deteriorated the mirror coatings so it became necessary to replace the mirrors. In addition, several epoxy bonds between the original mirrors and their mounts separated at low temperature. Alternate optomechanical mounting designs were attempted during the NASA GloPac (Hintsa et al., 2010) and MACPEX (Rollins et al., 2014) field missions, but did not provide adequate thermal stability at stratospheric temperatures below 240 K.

As reported in this paper, an entirely new optomechanical approach has been implemented for JLH Mark2 (see Sections 2 and 4). We also redesigned and ruggedized the instrument, developed new data retrieval algorithms and updated the calibration and data analysis procedures. These improvements in the new JLH Mark2 version of the instrument, along with recent field and laboratory performance are described in this paper. The rest of this paper is organized as follows. Section 2 provides an outline of the instrument. Instrumental issues in JLH Mark1 are described in Section 3 and improvements incorporated in JLH Mark2 are described in Section 4. Spectroscopy and data analysis are in Section 5. New performance specifications are in Section 6, followed by a summary in Section 7.

2. Instrument Overview

The JLH instruments are based on the detection of H_2O absorption in the 1370 nm wavelength region with an open-path multi-pass cell, as described previously (May, 1998). The light source is a commercial, narrow-linewidth, distributed feedback (DFB) tunable diode laser (TDL). The specific H_2O line targeted in JLH Mark2 atmospheric measurements has a linecenter wavelength of 1369.97 nm (7299.4311 cm^{-1}), as shown in Table 2. The total absorption pathlength is 10.479 m obtained by multi-passing the laser light between the mirrors of the open-path sample cell (Section 2.1). Examples of similar tunable laser hygrometers include the NASA LaRC Diode Laser Hygrometer or DLH (Diskin et al., 2002; Podolske et al., 2003), the Harvard Herriott Hygrometer or HHH (Sargent et al., 2013), the VCSEL hygrometer (Zondlo et al., 2010), and the SEALDH-II hygrometer (Buchholz and Ebert, 2018). A core set of hygrometers including JLH Mark1 were intercompared in the AIDA chamber at the Karhsruhe Institute of Technology in the AquaVIT-1 campaign (Fahey et al., 2014). A review of modern hygrometers is given in Bange et al. (2013).

The first flights of the newly improved JLH Mark2 were on the NASA ER-2 high-altitude aircraft in 2013 during the field mission for the NASA Studies of Emissions and Atmospheric Composition, Clouds and Climate Coupling by Regional Surveys (SEAC^{4}RS) (Herman et al., 2017). For these flights, JLH Mark2 was mounted in a camera port in the lower Q-bay of the NASA ER-2 fuselage (Figure 1a and Section 4). The ethernet-based NASA Airborne Science Data and Telemetry System (NASDAT) on the NASA ER-

https://doi.org/10.5194/egusphere-2024-4019
Preprint. Discussion started: 10 January 2025

2 aircraft (Sorenson et al., 2012) was used to acquire measurements and data that included time, GPS coordinates and static temperature/pressure from the Meteorological Measurement System (MMS; Scott et al., 1990).

Subsequently, JLH Mark2 flew on the Flying Test Bed (FTB) aircraft of the Northrop Grumman Corporation for contrail studies and flights of opportunity (2015-2023). For these flights, JLH Mark2 was mounted on top of the aircraft fuselage (Figure 1b). Northrop Grumman operates an Experimental Gulfstream II Test Bed aircraft (N82CR) used to assess mission system payloads prior to customer delivery. This aircraft is equipped with onboard equipment racks, electrical power dedicated to instrumentation, and external hardpoints for payloads. For this effort, an additional Total Air Temperature (TAT) probe, Goodrich P/N: 102DB1CK, was integrated. The selected probe is identical to the production Gulfstream II TAT probe and was mounted in a mirrored location compared to the production, i.e. same fuselage station, same waterline, but on the port side of the fuselage rather than starboard. The selected TAT probe is a dual mandrel design, 3-inches in length to measure outside the boundary layer, and heated with 28 VDC for de-ice. The probe was routed to an instrumentation system for data collection. Static pressure was also sampled. The airframe static pressure ports connect to Gulfstream Air Data Computers that drive an ARINC-429 data buss which is then displayed to the pilots. The ARINC signal was split and connected to mission-system computers so that static pressure was also collected for the payloads and instrumentation. An inertial navigation system (VectorNav P/N: VN-300) supplied position and time coordinates.

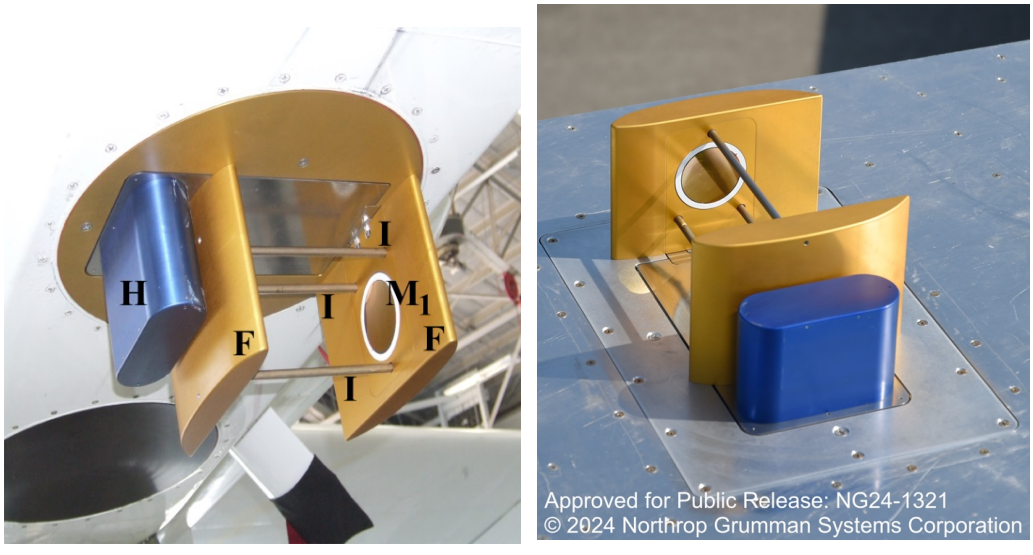

Figure 1: (Left) JLH Mark 2 mounted on a lower camera port underneath the NASA ER-2 fuselage Q-bay. The abbreviations used are H: evacuated housing for the tunable laser and detector; M1: the far plano-concave mirrors of the Herriott cell (the other mirror is hidden from view in this photo); I: three Invar rods used for maintaining the two mirrors at fixed separation (Section 3.1); and F: aerodynamic faring for deflecting the airflow around the mirrors of the Herriott cell, as described later in Section 4.2. (Right) JLH Mark 2 mounted above fuselage of NGC Gulfstream-II aircraft with the same JLH structure.

The JLH instrument payload ingested these temperature, pressure, and spatiotemporal data, providing water vapor mixing ratio at 1 Hz. For a limited number of flights, a commercial hygrometer (FLHYT P/N: WVSS-II) collected data simultaneously. Throughout the JLH campaign comprising 109 total flights, JLH data were collected at pressure-altitudes spanning 10, 000 ft to

https://doi.org/10.5194/egusphere-2024-4019
Preprint. Discussion started: 10 January 2025

45,000 ft (3000 m to 13,700 m), primarily in the daytime over the Isabella, Owens, and Bishop Military Operations Areas (MOAs) within the R-2508 complex in the Mojave Desert as well as a limited number of missions off the coast of Florida.

2.1 Optics

The optical open-path multipass absorption cell of JLH Mark2 is mounted external to the aircraft to avoid contamination or outgassing from surfaces (Figure 1a and 1b). The laser beam emerging from the TDL is collected by an aspheric lens and loosely focused at the midpoint of the multipass cell in the Herriott optical configuration (Altmann et al., 1981; Herriott et al., 1964). The multipass cell consists of two plano-concave mirrors made of Zerodur (lithium aluminosilicate glass-ceramic) substrate with their concave surfaces coated with gold to provide high reflectivity and an Al_2O_3 over-coating for protection. The mounting of the cavity mirrors in the Herriott cell is shown in the computer-aided design (CAD) drawing in Figure 2(a). The focused laser beam enters the cell through a small orifice in one of the mirrors M_0 (Figure 2(a)). The two mirrors (M_0 and M_1) are separated by 207.9 mm, have a diameter of 63.5 mm and radius of curvature of 219.66 mm. The angle at which the laser light is injected into the cell is such that the light travels fifty times between the mirrors before exiting the cell through the same orifice as the entrance beam. Upon exiting, it is focused onto a miniature InGaAs detector, located adjacent to the TDL. Both the laser and the detector are located inside an evacuated housing (H in Figure 1(a)), equipped with a transparent window. There is an additional 86-mm path through ambient air between the Herriott cell near mirror (M_0) and the window on the laser/detector housing, yielding a total optical path length of 10,479 mm (10.479 m). The TDL is mounted on a small aluminum plate, attached to a thermoelectric cooler (TEC) maintained at a specified temperature that is actively stabilized to ±0.01°C to minimize wavelength shift of the emitted infrared radiation.

https://doi.org/10.5194/egusphere-2024-4019
Preprint. Discussion started: 10 January 2025

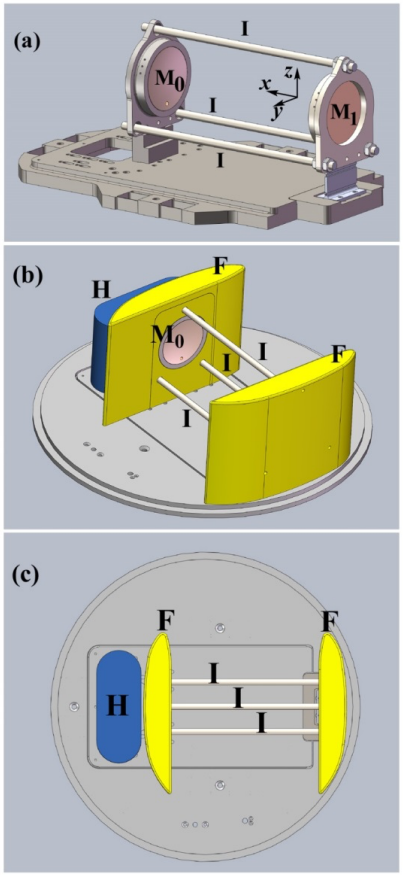

Figure 2: (a) CAD drawing of the JLH Mark2 Herriott cell consisting of two plano-concave mirrors, one of which (M_0) has a small orifice (barely visible at the bottom of M_0) through which the laser beam is injected at a specified direction. The beam undergoes 50 traversals between the mirrors and exits the cell through the same orifice (Section 2.1). The separation between the mirrors is fixed at a specified value by firmly attaching them to the ends of three Invar rods (I). Also shown are the x, y, z coordinates referred to in Section 4. (b) CAD drawing of the instrument showing two aerodynamic fairings (F) used for deflecting the airflow around the mirrors during flight, thus minimizing the distortion of airflow between the mirrors, as described in Section 4.2 (the direction of air flow is along y). H is an evacuated housing for the laser and the detector, and is equipped with an infrared-transmitting window. (c) CAD drawing of the top view of the instrument.

2.2 Instrument Electronics and Software

2.2.1 Basic Electronics

The JLH Mark2 electronics hardware includes a laser/detector pair for sensitive measurement of water vapor, the main JLH flight computer for laser control and signal processing, and an upgraded interface processor board (IPB) for onboard processing and network communication. The laser control and detector signal chain of JLH have been described previously in May (1998). Minor changes made to frequencies and implementation are described below. Figure 3 shows a block diagram of the laser control and signal processing electronics.

The laser current scan is produced uniquely by an audio codec integrated circuit in continuous direct memory access (May, 1998). The TDL is driven with a current sawtooth-shape ramp to scan across the water absorption feature at 8 Hz. The detection technique switches between second harmonic wavelength modulation and direct absorption measurement (Section 5). For direct absorption

https://doi.org/10.5194/egusphere-2024-4019
Preprint. Discussion started: 10 January 2025

measurement, the laser scan is measured directly in transmission mode (DC), with ten spectra co-added in software to save an averaged spectrum at 0.8 Hz. For harmonic detection, the audio codec digital-to-analog converters generate a small-amplitude sinusoidal waveform at frequency f = 128 kHz that is added to the sawtooth ramp. The detector signal is demodulated at frequency 2f = 256 kHz to yield the second harmonic spectrum.

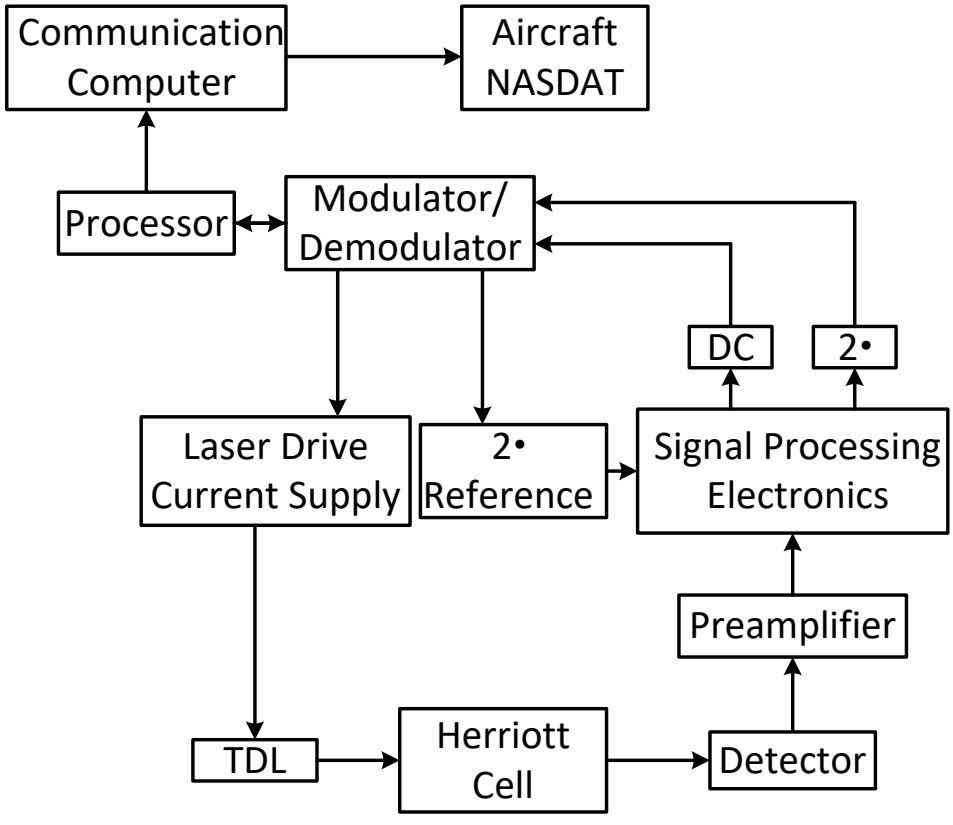

Figure 3: Block diagram of the electronics.

The flight computer is a legacy single-board computer (SBC) running the MS-DOS operating system (Ampro Corp.) with an 80486 microprocessor. The flight computer and electronics boards are in PC104 format, operating at +5 V DC and +12 V DC. Aircraft 28 V DC power is converted to +5 V and +12 V DC using dc-dc convertor modules (Vicor Corp.) with ripple attenuation, additional filtering, and overvoltage protection. Laser control and signal processing are carried out on a custom electronics board, and data are stored on a flash card.

The electronics are temperature-stabilized for greater accuracy and are maintained at 25° C by strip heaters (Minco Corp.) in pulse-width modulation mode (May, 1998). During flight, the aluminum heat-sink of the laser/detector pair is heated to 15° C by a commercial temperature controller (MPT 2500, Wavelength Electronics Corp.). For greater stability, the laser temperature is

https://doi.org/10.5194/egusphere-2024-4019
Preprint. Discussion started: 10 January 2025

further stabilized by a thermoelectric cooler (TEC) with active heating and cooling capability. The TEC is regulated by a temperature controller (Hytek 5640) that senses the temperature of a thermistor adjacent to the laser.

2.2.2 Changes to Electronics since JLH Mark1

To improve the signal-to-noise ratio and instrument stability, several changes have been implemented in JLH Mark2. Separate power supplies were installed for switching components (e.g., heaters and TEC) so that a dedicated low-noise power supply was used exclusively for the laser, detector, and computer. The signal chain was optimized for a narrow scan across the water absorption line at a pressure of 150 hPa (the most common flight altitude during the NASA SEAC^{4}RS field mission). In the signal chain gain stages, variable resistors have been replaced by precision fixed resistors to reduce noise. In addition, all cables and boxes have been shielded for electromagnetic field (EMF) protection.

JLH Mark2 incorporates a new interface processor board (IPB) running Red Hat Linux 2.4.7-10 to augment the I/O and on-board processing capability of the JLH legacy SBC. The processor is an AMD Geode GX466 (333 MHz) processor on a PC104 form-factor CoolLiteRunner (Lippert Corp.) SBC featuring two serial ports, 10/100BaseT Ethernet and 8 GB compact flash storage (WinSystems Corp.). The IPB forms the data interface between the JLH computer and the ethernet-based aircraft data system. On the NASA ER-2 aircraft, this data system is the NASA Airborne Science Data and Telemetry System (NASDAT); Sorenson et al., 2012), and on the NGC Flying Test Bed, the Vehicle Management Computer (VMC) collects all the data. One RS-232 serial port on the IPB is used to collect science telemetry packets transmitted by the main JLH processor. JLH packets consist of ASCII-encoded, comma separated values, terminated by linefeed character. After validating a packet receipt, values are converted from ASCII to binary. Data are time-stamped, stored on compact flash, formatted and transmitted as NASDAT-compliant UDP packets to the NASDAT. As part of the NASDAT, the ER-2 Linkmod forwards data packets to users on the ground. The IPB also collects pressure, temperature and standard aircraft housekeeping and navigational data in Interagency Working Group standard format number 1 (IWG1) to enable on-board real-time processing of JLH water vapor data. The IPB program, written in 'C', uses multi-threading to handle the asynchronous data streams.

2.2.3 Instrument Software

The legacy instrument software resides on the MS-DOS computer mentioned previously. It configures the hardware, continuously acquires the spectrometer data, and outputs a serial stream of raw data. The new communication software on the IPB then collects the serial output from the DOS computer and broadcasts it to the aircraft NASDAT or VMC. Upon receipt, the ground software processes the data “on-the-fly.” We provide more details on data analysis in Section 5.

The legacy instrument software has undergone minor upgrades since May (1998). It is written in C^{++} and operates as a single-threaded application in DOS. The basic data processing technique is similar to that of May and Webster (1993). The following are the user-selectable input parameters: laser scan rate, laser modulation frequency and depth, number of scans to be averaged, number of scans before the data are written to the flash drive, and the heater parameters. At the start of the program execution, the hardware, heaters and laser scan are initialized. In the next step, an infinite loop is initiated and data are acquired. In the timing sequence, shown in Figure 4, the TDL is first off for 3 ms to acquire the “null-point.” The laser scan ramp with a duration of 125 ms then turns the laser on and tunes the laser across wavelength region of interest. During the ramping, the laser is also modulated at a frequency f=128 kHz which is superimposed on the current ramp (Figure 4). The time-varying signal is detected at frequency 2f =

https://doi.org/10.5194/egusphere-2024-4019
Preprint. Discussion started: 10 January 2025

256 kHz and filtered by narrow band-pass filters to reduce the background. The peak-to-peak amplitude of the 2f spectrum is saved to disk along with laser power and other engineering parameters. After the ramp, the laser is turned off again for 3 ms to acquire a "null" signal. This on-off sequence is then repeated. The results from individual wavelength scans are averaged continuously by the software. As a compromise between the instrument precision and time resolution, 10 scans are averaged and mean data are reported every 1.28 s. Every ~20 s, the laser modulation is turned off and a direct absorption signal is acquired (again a 10-scan average).

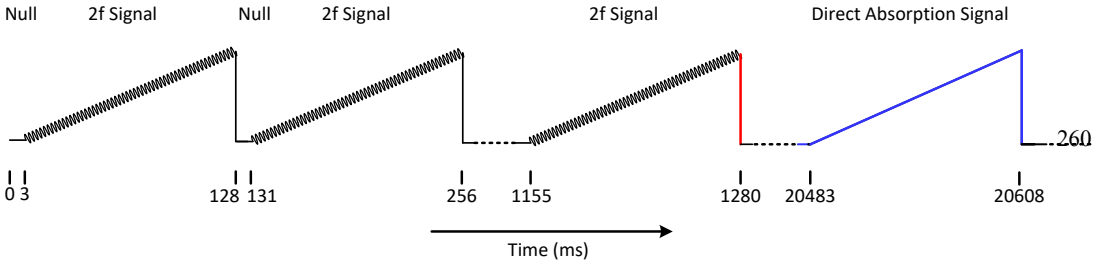

Figure 4: The data acquisition timing sequence (schematic, not to scale). Between t=0 and 3 ms, the scanning ramp is off and a "null signal" is acquired. At t= 3 ms, a ramp of 125 ms duration with a superimposed modulation is applied and the 2f signal is acquired (the modulation depth is exaggerated for clarity). The on-off sequence is repeated ten times until t=1280 ms, at which point (shown in red) ten 2f signals are averaged and a mean is reported. After the 160th cycle, at t~20 s, the laser modulation is turned off (shown in blue) and a direct absorption signal is acquired (again a 10-scan average, not shown here).

The new communication software transmits real-time data to the aircraft data system (Section 2.2.2). The ground software processes the broadcasted data stream from JLH (spectroscopic data) and pressure and temperature (provided by MMS on the NASA ER-2, and facility sensors on the FTB). Water mixing ratios are calculated using the algorithms of May and Webster (1993). Measured peak-to-peak 2f (pp2f) amplitude is compared with a look-up table of expected pp2f as a function of pressure and temperature. The expected pp2f is interpolated between the table values of the nearest pressure and temperature to calculate the mixing ratio of H_2O (May, 1998).

2.3 Calibration

2.3.1 Laser Calibration

The laser parameters of interest are wavelength, spectral purity, linewidth, tuning rate, and laser modulation amplitude. We first determine the absolute laser wavelength to within ~0.18 nm (1 cm^{-1}) with a Burleigh wavemeter. The wavelength is then refined by using five identified spectral lines of CH_4 in the same spectral region as the water line of interest for calibration. For this purpose, measurements are made with JLH Mark2 in a laboratory test chamber containing low-pressure methane with a small amount of water vapor. The methane line positions are known to within 0.0001 cm^{-1} (Brown et al., 2013), allowing the accurate determination of the water line positions by interpolation. The spectral purity of the laser is verified by measuring the laser transmission through a sample at very high water vapor concentrations, which absorbs all the light at the line center wavenumber of 7299.4311 cm^{-1}. The laser linewidth is determined in the laboratory by measuring the water absorption lineshape at low pressures where the absorption linewidth is solely due to the Doppler width. If the line is wider than the predicted Doppler width, it is assumed to be a convolution of the laser linewidth and Doppler width (Section 5). The laser tuning rate is determined in the laboratory by using the CH_4 lines adjacent to the water line as wavelength standards.

https://doi.org/10.5194/egusphere-2024-4019
Preprint. Discussion started: 10 January 2025

For very sensitive detection with second harmonic detection in wavelength modulation spectroscopy (May and Webster, 1993; May, 1998), the laser wavelength is also modulated in addition to being tuned by superimposing a small sinusoidal modulation at a frequency f=128 kHz on the tuning ramp. The modulation amplitude is optimized for maximum second harmonic peak-to-peak signal from a water line that is pressure-broadened at 150 hPa total pressure. The modulation amplitude is set by the user in electrical units (mA laser current). It is critical to know the actual modulation amplitude in spectroscopic units (wavenumbers, cm^{-1}). This is determined in the laboratory by placing JLH Mark2 inside a continuous flow chamber (Section 2.3.2), measuring well-characterized water mixing ratios over a range of pressures from 100 hPa to 700 hPa, and comparing the JLH Mark2 signal to synthetic modulated spectra. This method of estimating laser modulation is described by May and Webster (1993).

2.3.2 Spectrometer Calibration

The instrumental parameters of interest are the optical pathlength in the multipass absorption cell and the instrument response (sensitivity). The optical pathlength is checked in the laboratory by individually identifying each pass of the laser light between the mirrors with an infrared detection card, covering and uncovering each spot on the near and far mirrors. The fraction of light impinging on the detector from the final reflected pass (as opposed to an adjacent pass) has been measured to be greater than 99.9%.

The instrument response is characterized through measurements on a standard sample with known water mixing ratio (see below). This is then compared with the water mixing ratio obtained by using the HITRAN database (Rothman et al., 2013). The ratio of the two is used as the instrument response factor and is used to scale the field measurements. This effectively cancels out the errors due to uncertainties in the line strength in the HITRAN database.

By 2007, improved calibration methods were developed, which allowed for laboratory measurements of sample atmospheres in test chambers with water volume mixing ratios as low as 2 parts-per-million by volume (ppmV) (Troy, 2007). The source of the air-water mixture for determining the instrument response mentioned above is the commercially available Thunder Scientific 3900 low-humidity generator (http://www.thunderscientific.com/humidity_equipment/model_3900.html), which can provide air with stable water mixing ratios from less than 1 ppmv to 12,000 ppmv. The carrier gas is ultrazero air from cylinders. The Thunder Scientific 3900 uses a technique that generates air with a constant water mixing ratio to an accuracy of 0.1 K frostpoint (corresponding to better than 1% accuracy of mixing ratio). The technique is a primary standard recognized by NIST and used by commercial hygrometer manufacturers to check their instruments. It depends solely on accurate measurements of pressure and temperature to achieve a constant mixing ratio of water vapor in air flowing over a saturator. For calibration of the JLH instrument in the lab, the sampled air mixture is checked both upstream and downstream of JLH with a reference Vaisala DM500X precision surface-acoustic wave (SAW) hygrometer. Typically, half of the flow is directed through JLH and the rest through the Vaisala hygrometer, which has a quoted accuracy of 0.3 K frostpoint (corresponding to 2% accuracy of water mixing ratio).

2.4 Instrument mounting on aircraft platforms

Over the years, the JLH instruments have been mounted on various locations on scientific aircraft. Examples include lower camera ports underneath the NASA ER-2 wing pod (May, 1998) and ER-2 Q-bay (Figure 1a), hatches underneath the wing of the NASA WB-57F aircraft, and most recently the fuselage of the Northrop Grumman Corporation FTB (Figure 1b). The airflow is the free-stream flow across the instrument between the mirrors, which are farther away from the aircraft than the estimated boundary layer.

https://doi.org/10.5194/egusphere-2024-4019
Preprint. Discussion started: 10 January 2025

There is no sample inlet or outlet in the conventional sense and the sample is constantly flowing across the instrument axis. The sample replenishment time is estimated to be ~0.3 millisecond across the optical path, assuming an air speed of 200 m/sec. Computational fluid dynamics calculations for the WB-57 aircraft indicate that the pressure and temperature at the mounting location are not significantly different from ambient values, within the uncertainties of the in-situ static pressure and static temperature measurements (Engblom, 2003). The open-path cell and its location on the aircraft ensure accurate water measurements without wall-effect contamination, especially in ice super saturated air and contrails.

3. Design issues in JLH Mark1

3.1 Optomechanical stability

The original JLH Mark1 instrument was designed and built in the early 1990s, and flew for over a decade in its original configuration (May, 1998). With the accumulation of years of flight data, it became clear that the JLH instrument needed redesign and upgrades due to some inherent design weaknesses, and also due to wear and deterioration of the instrument from years of use.

Design weaknesses in the original JLH resulted in thermal instability of the optics over the wide range of temperatures (180 to 300 K) experienced during airborne field missions. This caused loss of light intensity at the detector as the instrument temperature decreased with altitude. Due to temperature induced distortions of the optical bench and mirror holders, the laser beam path would shift until a portion of the beam would not impinge upon the detector. Because the laser / detector system measures the ratio of laser power while tuning across the water absorption line to the laser power off-line, the instrument is self-normalizing to a certain extent. However, with signal strength loss due to beam drift and reduced mirror reflectivity due to wear and deterioration, the signal-to-noise ratio would decrease. This eventually became a limiting issue in the NASA MACPEX campaign in 2011 (see Table 1).

A major problem with the original optical bench design was that it was structurally over constrained. The optical bench was constructed from materials that had markedly different coefficients of thermal expansion (CTE). As the instrument temperature decreased with altitude, the materials contracted by different amounts, pressed against each other, and induced high stresses. This caused distortion of the optical bench. For example, the original JLH design for the Herriott cell consisted of two spherical mirror holders rigidly held by three Invar rods. This Herriott cell assembly was rigidly bolted to a flat plate made of G-10 fiberglass. As the temperature of this system decreased, the Invar rods experienced very little contraction, whereas the G-10 plate shrank by almost two orders of magnitude more than the Invar rods. This caused the entire optical bench to distort and impressed forces of several hundreds of Newtons onto the Herriott cell. The solution to this problem was to redesign the optical bench so that all components were kinematically mounted (Section 4.1).

3.2 Laser stability

The JLH Mark1 instrument originally used a TDL that sampled the 7294.1229 cm^{-1} water line. The replacement laser was suitable for only sampling the H_2O line at 7299.4311 cm^{-1}. This meant that a new water absorption line was being measured, requiring fresh instrument calibration. However, from a spectroscopic perspective, this was a better line because of a smaller temperature-dependence (arising from slightly higher ground-state energy for the new water line). In addition, the 7294.1229 cm^{-1} line is flanked by two weak water lines, thus slightly complicating the analysis. The 7299.4311 cm^{-1} line, on the other hand, is easier for data processing because it is isolated from other water lines.

https://doi.org/10.5194/egusphere-2024-4019
Preprint. Discussion started: 10 January 2025

4. Improvements implemented in JLH Mark2

4.1 Optomechanical redesign

For the new optomechanical design of JLH Mark2, we used kinematic mounting to improve instrument stability. In kinematic mounting, an instrument, or an element of an instrument, is mounted such that each of its six degrees of freedom (DOF) is constrained non-redundantly by the mountings; there are only six physical constraints that uniquely control the six DOF. True kinematic mounting prevents any forces from being induced between any of the mounted components. Approaching ideal kinematic mounting becomes very difficult and expensive in real physical systems due to non-ideal components experiencing distortion and friction at very small scales due to applied forces. However, there are methods of design by which the induced mounting forces can be minimized at the constraints such that effect upon the mounted system is negligible. This is referred to as quasi-kinematic, or semi-kinematic, mounting. In engineering documentation, when a mounting system is referred to as kinematic, it is usually a reference to a quasi-kinematic mounting system; we use that meaning for kinematic here. For a more detailed exposition of these principles, see Yoder (2008).

To address the stability issues noted in Section 3.1, a combination of materials selection and kinematic design were used. The new design has the M_0 mirror in the Herriott cell mounted rigidly to a steel plate, as shown in Figure 2. The change was made from G-10 fiberglass to steel to increase strength and resistance of flexure of the system due to vibration. 15-5 PH steel was used due to its low CTE; the CTE is on the order of 60% of many other steels. The M_0 mount constrains motion of the Herriott cell in all six DOF. The M_1 mirror is attached to the steel plate using a spring mounting, or flexure. This flexure constrains the M_1 mirror in five DOF. The M_1 mirror is allowed to move along the x axis, resisted by a very low spring force. If the M_1 mirror were also rigidly mounted, the constraint of the x degree of freedom would be redundant, and forces would arise between the mirrors as the temperature of the instrument changed, which would cause distortions in the system. Instead, because of the flexure mount, as the temperature decreases and the steel plate contracts, the M_1 mount flexes in the x direction and a force of only 22 Newtons is applied along the Invar rods between the two mirror holders. The force is not zero, but it is two orders of magnitude less than in the original, non-kinematically, mounted JLH Mark1 Herriott cell.

The steel optical bench plate is mounted to an aluminum adapter plate, which is, in turn, mounted to an aircraft structure. The adapter plate is used so that JLH Mark2 may be mounted on multiple airframe structures. As most aircraft structures are made of aluminum, there is a CTE match and the adapter plate can be bolted directly to the aircraft with no need for flexural mounts. Because of the difference in CTE between the steel and aluminum, the optical bench itself is mounted to the aircraft adapter plate using three flexures.

Within the Herriott cell, the mirror holders, which are made of Invar, are connected by three screws to the mirror mounts, which are made of titanium. Two of the three screws clamp the mirror holders to small flexures in the titanium mounts. This prevents stresses arising between the mounts and the mirror holders across the span where the two materials of dissimilar CTE are clamped together. The mirrors, which are made of Zerodur (a glass-ceramic with very low CTE) are held in the mirror holders by three pads of high strength silicone adhesive. The silicone pads act as flexures that prevent buildup of stresses between the mirrors and the mirror holders.

https://doi.org/10.5194/egusphere-2024-4019
Preprint. Discussion started: 10 January 2025

4.2 Aerodynamic fairings

The authors considered aerodynamics in the redesign of JLH Mark2 to minimize distortion of the airflow in the optical path of the external Herriott Cell, and to improve stability. The new design features aerodynamic fairings resembling stubby wings that maintain a constant air density between the mirrors. In JLH Mark1, these fairings had the form of symmetric ellipsoidal airfoils (May, 1998). That Mark1 configuration with a pair of airfoils would create a venturi effect, thus accelerating the flow between the two fairings. The associated pressure reduction is expected to cause a reduction in air density precisely where the instrument measures absolute water content. The final specific moisture content would thus be erroneous because it is computed using the free-stream value of air density. In addition, the JLH Mark1 airfoils experience significant deflection during flight.

In the modified JLH Mark2, we designed new fairings to overcome the above issues. We reshaped the fairings using cambered airfoils to keep the air density between the two fairings equal to the free stream density, which is equivalent to having a pressure coefficient of zero in the region between the two fairings. This also implies that all of the air approaching the leading edge of the fairings needed to be deflected around the top surface of the airfoil. Here, we are using "top" and "bottom" in relation to the usual orientation of wings on airplanes. These fairings are not horizontal when mounted as part of the instrument. It was reasoned that since these fairings do not disturb the flow going underneath them, two identical such fairings could be placed with their bottoms facing one another and that the flow around each would behave independently of the other. In other words, two identical airfoils could be used and the flow around them would not interact. This simplified the aerodynamic analysis by not having to treat the two wings as being part of a biplane. This lack of interaction between the two fairings has not been proven, but it was simply assumed to be true and the airfoil shape was then developed in isolation.

There were some constraints on the shape of the airfoil besides the goal of achieving a pressure coefficient close to zero on the lower surface. The physical mounting required the instrument to fit through a hole in the surface of the aircraft, the 50.8 cm diameter camera port in the lower Q-bay of the ER-2 aircraft. That space constraint limited the extent of the airfoil upper surface. This mounting constraint also prevented a long tapered trailing edge, resulting in a rather steep aft surface. The fairings, of course, had to provide sufficient room inside them for the Herriott cell mirrors that they are intended to protect. They also had to accommodate a small amount of adjustability in the spacing between the two mirrors. In order to simplify machining, alignment and mounting of the two fairings, we kept a large portion of the bottom surface flat (similar to the Clark Y airfoil). A similar self-imposed constraint was to construct the shape of the airfoil using only circular arcs and keeping them tangent at the transition points from one arc to the next. The pressure distribution on the airfoil was computed using XFOIL, a powerful, free, two-dimensional flow solver developed by M. Drela at MIT (Drela, 2013). The final shape developed here was the result of only four iterations. Treating the airfoils as two-dimensional means that we implicitly neglected any effects due to trailing wingtip vortices. Given the low aspect ratio of these stubby wings, there must be some spanwise flow towards the tips in the region between the two fairings. We did not make any attempt to quantify the impact of this effect. Figure 5 shows the final shape of the fairing and Figure 2 shows the 3-dimensional CAD drawing of the fairings in the JLH Mark2 instrument.

In addition to the aerodynamic improvements, the JLH Mark2 design isolated the Herriott cell system from the airflow management system of the fairings. The JLH Mark1 design had the mirrors mounted directly to the airfoils, which were, in turn, mounted directly to the optical bench plate. In addition to the cell distortion issues due to the structural over constraints, deflections due to aerodynamic loads on the airfoils affected the mirrors. The JLH Mark2 design eliminated this issue by making the Herriott cell and the fairings independent systems. The Herriott cell and the fairings are both mounted to the optical bench, but there is no

https://doi.org/10.5194/egusphere-2024-4019
Preprint. Discussion started: 10 January 2025

physical contact between them. In this way, the Herriott cell is isolated from any distortions and vibrations of the fairings due to aerodynamic loads.

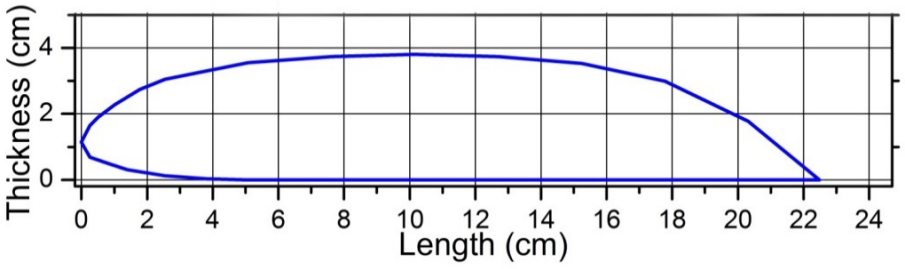

Figure 5: Airfoil shape for zero coefficient of pressure on much of the lower surface.

5. Data Analysis

The data reduction technique follows closely on May (1998) and May and Webster (1993). The accuracy of the water concentration obtained from JLH Mark2 measurements is limited primarily by uncertainties in the laser parameters and spectral fitting. In the section below we describe the steps to measuring the parameters needed for accurate water vapor measurement.

In the laboratory, the laser tuning rate is determined by fitting to low-order polynomial of multiple CH_4 lines surrounding the targeted H_2O line (Section 2.3.2). The instrument line-shape is then characterized by comparison of a low-pressure absorption feature with the expected profile of a Doppler line-shape. Figure 6 shows an experimental line shape obtained with the Herriott cell in a laboratory test chamber at a temperature of 297.54 K with pure water vapor at a pressure of $9x10^{-2}$ hPa. The observed absorptance, $(I-I_o)/I$, is only ~0.134, so the sample is optically thin and the line shape is due to only Doppler broadening. The Gaussian fit shown in Figure 6 yields a half width at half maximum of 0.01085 cm^{-1}. If the Gaussian is a convolution of Doppler-broadened linewidth and laser linewidth, then we calculate an effective instrument linewidth of 0.00217 cm^{-1} (65 MHz), close to the value observed in JLH Mark1 measurements at 7294.1229 cm^{-1} (May, 1998). We believe the observed instrument linewidth is a convolution of the true laser linewidth (which is much less) and the somewhat slow response of the electronics. Tunable DFB diode lasers usually have a half width of ~5-20 MHz. Preliminary observations suggest that the response of the electronics is indeed slow, contributing to the observed somewhat large effective instrument linewidth.

JLH Mark2 uses a combination of fast 2f spectra and less-frequent direct absorption spectra to calculate water vapor mixing ratios. As described in Section 2.3.3, 2f spectra are acquired at 8 Hz, and averages of 10 harmonic spectra are written to the flight computer for real-time communication to the ground and subsequent analysis. Figure 7 shows one such raw second-harmonic (2f) spectrum (black trace) in the stratosphere during a flight on 2 September 2013. The blue trace is the return laser power at the detector. At index 44, the laser power drops to its zero level (with a very small contribution from background light) during the 3-msec laser off period, described in Section 2.2.3. The laser power increases with applied current as the index increases. We note that this is a stratospheric measurement with less than 10 ppmV water vapor. At such low concentrations, direct absorption signals are very

https://doi.org/10.5194/egusphere-2024-4019
Preprint. Discussion started: 10 January 2025

485 weak and the observed 2f signal shown here is a testament to the high detection sensitivity possible in wavelength modulation spectroscopy.

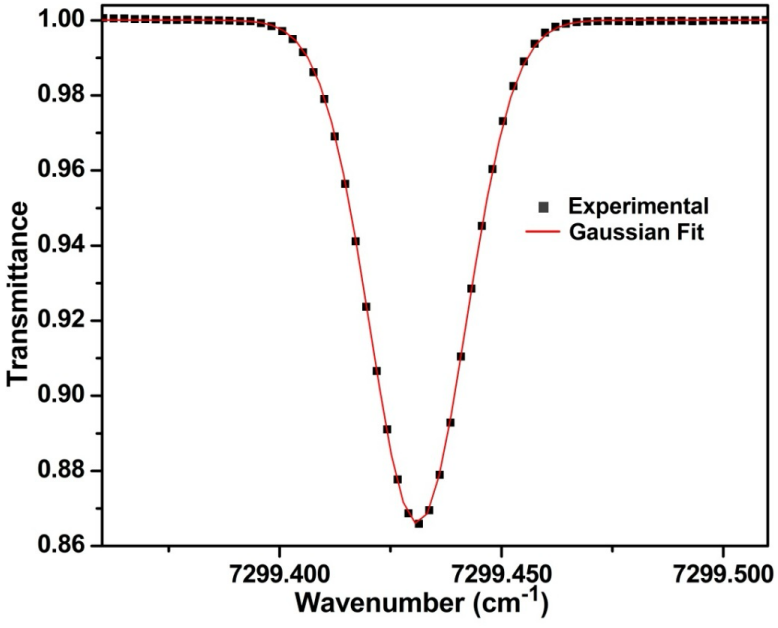

Figure 6: Experimental transmittance spectrum and a Gaussian fit to the data, where the transmittance = 1- absorptance.

https://doi.org/10.5194/egusphere-2024-4019
Preprint. Discussion started: 10 January 2025

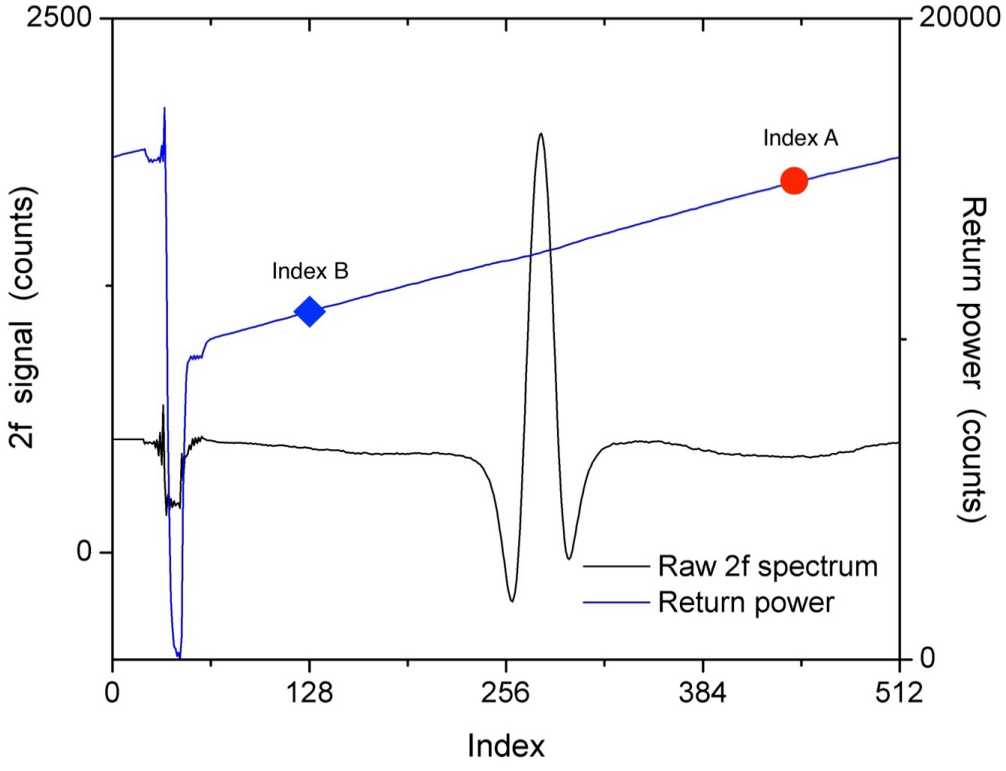

510 **Figure 7: An example second harmonic (2f) spectrum (black trace) and return laser power spectrum (blue trace) acquired with JLH Mark2 during the NASA ER-2 aircraft flight of 2 September 2013. The spectrum was recorded at 82178 sec UTC at a pressure of 129.96 hPa, temperature of 203.3 K and a calculated water volume mixing ratio of 6.81 ppmV. As reference for Figure 9, the return laser power is identified at two points, the blue diamond is Index B and the red circle is Index A.**

515

The 2f signal has a characteristic second-derivative type shape with two negative lobes and one positive lobe at the line-center. The second negative lobe is truncated due to limited time response of the signal chain. For JLH Mark2 measurements, the peak-to-peak 2f amplitude (pp2f) is measured between the first negative lobe and the positive lobe. This measurement is precise, but not
520 as accurate as direct absorption. The 2f baseline is curved due to a Fabry-Perot interference fringe from a short back-reflection in the optical system.

At higher water vapor concentrations, direct absorption measurements are more accurate. Every 28 seconds, the laser modulation is turned off to record a direct absorption spectrum (ten-scan average) as mentioned in Section 2.3.3. An example of such a spectrum
525 is shown in Figure 8, acquired during a NASA ER-2 aircraft flight of 2 September 2013. Also shown is a fitted Voigt lineshape.

In our analysis, we obtain the water concentration by comparing the observed line-shape with that calculated by using the spectroscopic parameters in the HITRAN database. Laboratory calibration with a reference source is then used to verify this

https://doi.org/10.5194/egusphere-2024-4019
Preprint. Discussion started: 10 January 2025

approach. The advantage of direct absorption spectroscopy is that it is ratiometric – absolute concentrations are inferred from ratios of signals at different wavelengths (along the line profile) without the need to calibrate a scalar quantity representing the system signal gain, such as pp2f amplitude in 2f-spectroscopy. Consequently, direct absorption measurements are more accurate than 2f measurements. This methodology is considered "calibration free" because of its first principles approach. This methodology has been assessed by comparing the results with a national humidity standard (Buchholz, 2014; Buchholz and Ebert, 2018). For the absorption shown in Figure 8, our analysis yields a water vapor concentration of 296 ppmV.

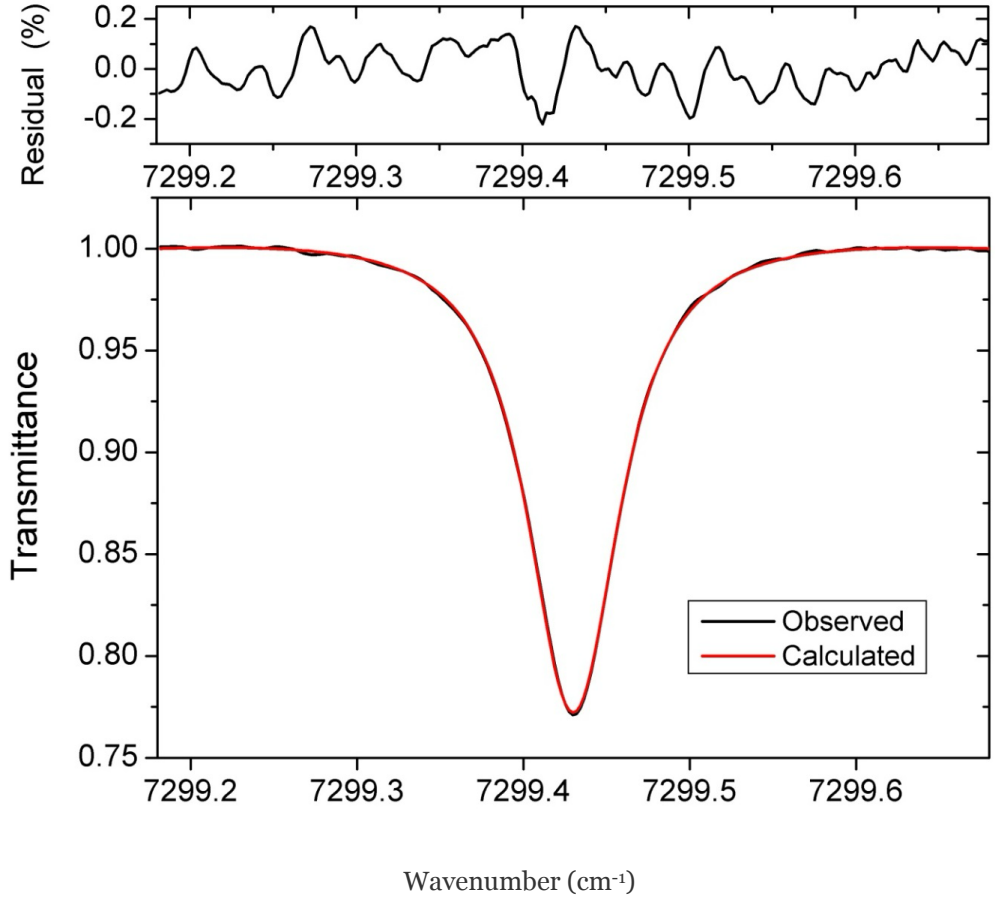

Figure 8: A high ambient pressure transmission spectrum during a flight on Sept 2, 2013, at a pressure of 225.95 hPa (169.48 Torr) and a temperature of 225.19 K. Also shown is a fitted spectrum, yielding a water concentration of 296 parts-per-million by volume (ppmV).

The residuals in the upper panel in Figure 8 demonstrate that the fits are generally good and that spectral fitting residuals are generally within JLH noise level. However, we caution that there are errors originating from the assumed line-shape function and the line parameters, often contributing to retrieval errors. The Voigt function assumed for air-broadened lines in our spectral analysis programs can lead to error on the order of 2%.

https://doi.org/10.5194/egusphere-2024-4019
Preprint. Discussion started: 10 January 2025

6. Performance

6.1 Measured improvement in precision and optical stability

JLH Mark2 has significantly steadier return laser power than previous optical configurations of JLH Mark1 (Mark1a and 1b). To prepare for airborne measurements, we tested JLH Mark2 in a low-temperature chamber (Cincinnati Sub-Zero Z-Plus Temperature/Humidity Chamber) at temperatures as low as 203 K and verified stable optics. The JLH Mark2 instrument then flew as part of NASA SEAC^{4}RS and the NGC FTB flights. Example data tracking return laser power during a single FTB flight in the UTLS are shown in Figure 9. Indices A and B (as shown in Figure 7) were selected to be in non-absorbing regions on either side of the water feature and thus reflect only return laser power at a given injection current. Note that the DC gain was deliberately reduced between SEAC^{4}RS (Figure 7) and FTB (Figure 9), so the signal from return laser power is proportionately lower on FTB flights. Figure 9 illustrates that, over the static temperature range of 197 – 233 K, return laser power varies only 0.7% and 1.1% for indices A and B, respectively. Matching trends between the two indices shows that power variation is constant across a given laser scan, which is easily accounted for in the signal processing. Given that laser alignment and return power is optimized at room temperature, the observed increase in power with decreasing temperature suggests that misalignment and optical losses are not dominant and are no longer a limiting factor in instrument performance. Instead, thermal drift of the laser is the dominant factor where lower laser temperatures result in increased output power at a given injection current. This laser drift may be caused by temperature drift of the heat sink or drift of the laser current-generating chip itself.

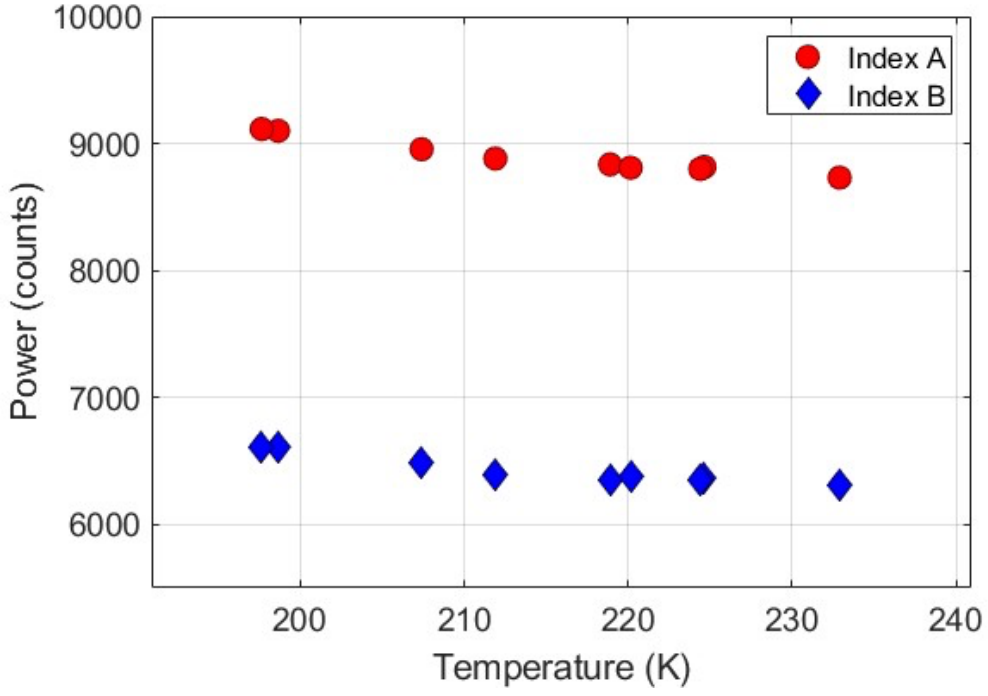

Figure 9: The redesigned optical mount maintains stable return laser power over the entire range of UTLS temperatures (190-240 K). Index A (red circles) and Index B (blue diamonds) are the same as in Figure 7. Data from NGC FTB flight of January 13, 2021.

https://doi.org/10.5194/egusphere-2024-4019
Preprint. Discussion started: 10 January 2025

The precision of JLH Mark2 is also better than JLH Mark1a and 1b. May (1998) reported 0.050 measurement ppmV precision for water concentration measured by JLH Mark1a. In practice, the JLH Mark1 precision deteriorated from year to year as the mirror reflectivity decreased due to environmental degradation. For comparison, we show the performance of JLH Mark2 during the SEAC^{4}RS field mission in Figure 10. The stratospheric precision of JLH Mark2 was 0.015 ppmV, which is to 0.4% of the water volume mixing ratio (3.82 ppmV).

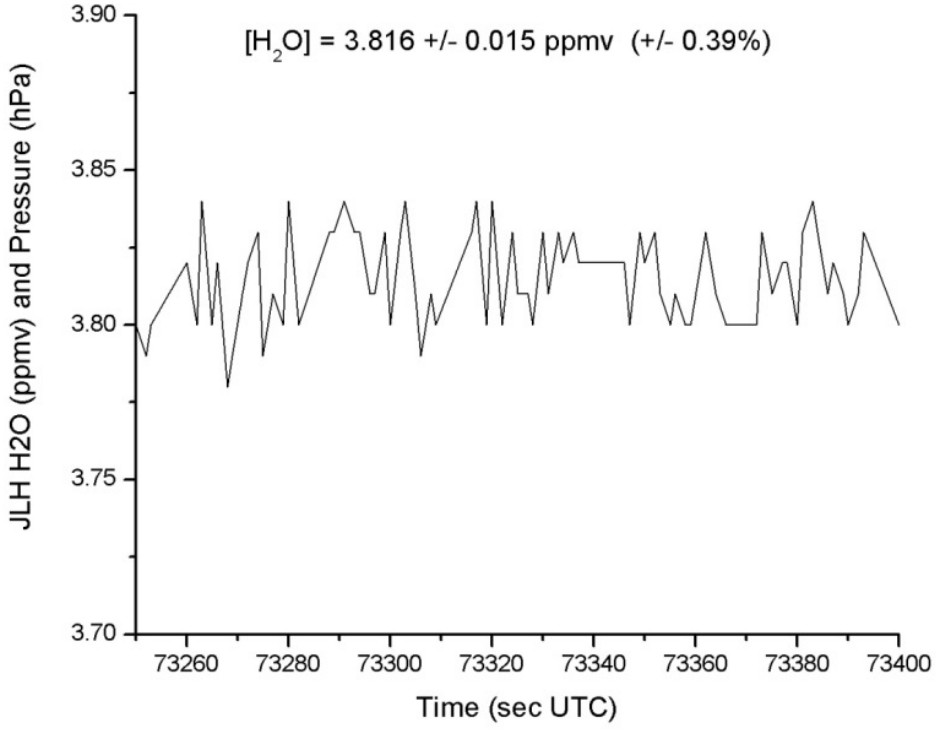

Figure 10: Stratospheric water measurements during level flight of the NASA ER-2 aircraft on 8 Aug 2013 recorded by JLH Mark2. In this flight segment, water vapor is expected to be nearly constant. The standard deviation of the measurement is 0.015 ppmV.

6.2 Comparison with other instruments

In 2007, JLH Mark1 participated in the AquaVIT-1 laboratory intercomparison of hygrometers (Fahey et al., 2014). For this multiweek campaign, the AIDA chamber was utilized as a uniformly mixed reservoir of constant water vapor mixing ratio over a range of pressures and temperatures. The core of the JLH instrument (multipass cell and laser/detector) were installed within the AIDA chamber. The benefit of installation inside the chamber was that pressure, temperature, and humidity were stable and well-characterized. A fan circulated the air to ensure uniformity. More importantly, the range of pressures, temperatures, and water inside the chamber were very similar to what JLH experiences during aircraft measurements in UT/LS field missions. The value of the AquaVIT experiment was that many of the world's leading in-situ atmospheric hygrometers simultaneously measured a common source of trace water in air, and submitted data to a blind intercomparison. Close agreement was found between

https://doi.org/10.5194/egusphere-2024-4019
Preprint. Discussion started: 10 January 2025

instruments, in particular JLH, the Cryogenic Frostpoint Hygrometer (CFH; Voemel et al., 2007) and the AIDA facility diode laser (APicT; Ebert et al., 2005) measured water vapor within 10% over a wide range of temperatures (195 K to 243 K). This validates our approach to measuring water vapor with an open-path spectrometer, and the accuracy of the spectroscopy over a wide range of temperatures.

As part of the NGC FTB flights, a a commercial hygrometer (FLHYT P/N: WVSS-II) accompanied JLH Mark2 on the flight of March 20, 2015. Figure 11 shows a comparison between the two instruments during an aircraft descent over Lancaster, California. Although the instruments have different time resolutions, the measurements are in general agreement to within 10%. Detailed intercomparisons with other hygrometers will be the subject of an upcoming publication.

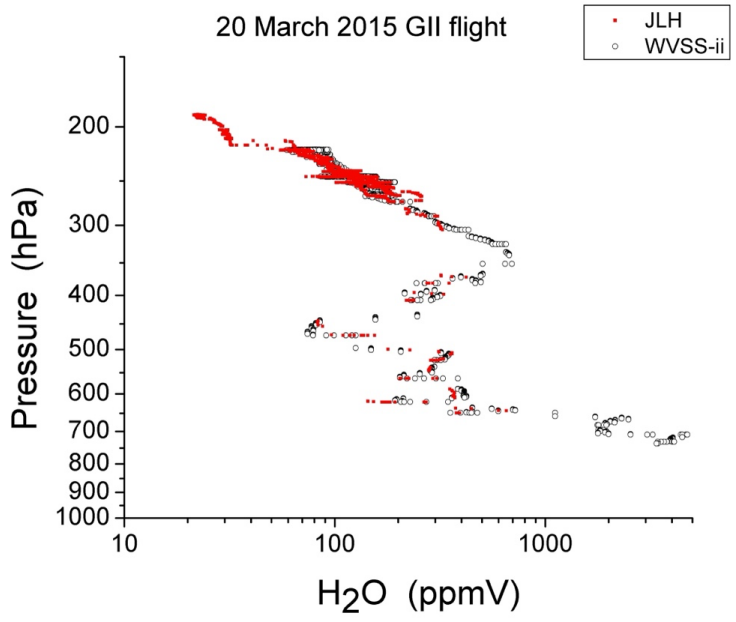

Figure 11: Water vapor profiles from JLH Mark2 and WVSS on March 20, 2015, during a NGC FTB flight.

7. Summary

This instrument paper reports the redesigned opto-mechanical structure of the JLH Mark2 instrument, new data retrieval algorithms, and updated data analysis procedures. The mechanical redesign has significantly improved the optical stability of the instrument. We have demonstrated that misalignment and optical losses are not dominant and are no longer a limiting factor in instrument performance. JLH Mark2 has improved precision of water vapor measurements compared to earlier versions of the instrument. We present this kinematic design as an inherently stable design for atmospheric sensors that are exposed to a wide range of temperatures.

Data availability. The SEAC^{4}RS aircraft data used in the data analysis can be freely downloaded from the following Digital Object Identifier (DOI): SEAC4RS doi:10.5067/Aircraft/SEAC4RS/Aerosol-TraceGas-Cloud. We expect the NGC data to be publicly released by June 2025. Files are available from corresponding author Robert Herman upon request: Robert.L.Herman@jpl.nasa.gov.

https://doi.org/10.5194/egusphere-2024-4019
Preprint. Discussion started: 10 January 2025

Author contributions. Robert Herman prepared the manuscript with contributions from all coauthors and was responsible for all aspects of the JLH Mark2 as principal investigator. Robert Troy designed the mechanical structure and athermal optimal mount of JLH Mark2 and contributed the Optomechnical section of this paper, Kim Aaron designed the air foils, Isabelle Sanders and Kevin Schwarm performed the data analysis of power stability. Eric Klobas and Aaron Swanson managed the NGC science and provided merged data sets from NGC FTB flights, Andrew Carpenter managed the NGC FTB and contributed its description in this paper. Scott Ozog collected and processed data from NGC FTB flights. Keith Chin and Robert Stachnik operated the JLH Mark2 instrument in the field and downloaded data post-flight. Dejian Fu, Robert Stachnik, Keith Chin and Lance Christensen developed software components for the JLH Mark2 instrument and/or its data reduction. Ram Vasudev contributed to the spectroscopy section of this paper.

Competing interests. The authors declare that they have no conflict of interest.

Acknowledgements

We thank Chris Webster, Gregory Flesch, Robert Jarnot, and James Margitan for helpful discussions. We thank Jose Landeros and Dave Natzic for circuit assembly, cable assembly and technical support in the laboratory and field, and the aircraft crew and flight planners for making these measurements possible. We thank Kamjou Monsour for characterizing diode lasers for this project. Part of this research was performed at JPL, California Institute of Technology, formerly under a contract with NASA and more recently under a Space Act Agreement contract with Northrop Grumman Corporation and NASA.

References

Altmann, J., Baumgart, R., and Weitkamp, C.: Two-mirror multipass absorption cell, Appl. Optics, 20, 995-9, 1981.

Anderson, J. G., Wilmouth, D. M., Smith, J. B., and Sayres, D. S.: UV Dosage Levels in Summer: Increased Risk of Ozone Loss from Convectively Injected Water Vapor, Science, 337(6096), 835-839, 2012.

Bange, J., Esposito, M., Lenschow, D. H., Brown, P. R. A., Dreiling, V., Giez, A., Mahrt, L., Malinowski, S. P., Rodi, A. R., Shaw, R. A., Siebert, H., Smit, H., and Zöger, M.: Measurement of Aircraft State and Thermodynamic and Dynamic Variables, Chapter 2 in Airborne Measurements for Environmental Research, Wendisch, M., and J.-L. Brenguier, ed., Wiley Series in Atmospheric Physics and Remote Sensing, Wiley-VCH Verlag, Weinheim, Germany, 7-74, 2013.

Boone, C. D., Walker, K. A., and Bernath, P. F.: Speed-dependent Voigt profile for water vapor in infrared remote sensing applications, J. Quant. Spectros. Rad. Trans., 105, 525-532, 2007.

Boucher, O., Randall, D., Artaxo, P., Bretherton, C., Feingold, G., Forster, P., Kerminen, V.-M., Kondo, Y., Liao, H., Lohmann, U., Rasch, P., Satheesh, S. K., Sherwood, S., Stevens B., and Zhang, X. Y.: 2013: Clouds and Aerosols. In: Climate Change 2013: The Physical Science Basis. Contribution of Working Group I to the Fifth Assessment Report of the Intergovernmental Panel on Climate Change [Stocker, T. F., Qin, D., Plattner, G.-K., Tignor, M., Allen, S. K., Boschung, J., Nauels, A., Xia, Y., Bex, V., and Midgley, P. M. (eds.)], Cambridge University Press, Cambridge, United Kingdom and New York, NY, USA, 2013.

https://doi.org/10.5194/egusphere-2024-4019
Preprint. Discussion started: 10 January 2025

Brown, L.R., Sung, K., Benner, D.C., Devi, V.M., Boudon, V., Gabard, T., Wenger, C., Campargue, A., Leshchishina, O., Kassi, S., Mondelain, D., Wang, L., Daumont, L., Régalia, L., Rey, M., Thomas, X., Tyuterev, Vl.G., Lyulin, O.M., Nikitin, A.V., Niederer, H.M., Albert, S., Bauerecker, S., Quack, M., O'Brien, J.J., Gordon, I.E., Rothman, L.S., Sasada, H., Coustenis, A., Smith, M.A.H., Carrington, Jr, T.,.Wang, X.-G, Mantz, A.W., Spickler, P.T.: Methane line parameters in the HITRAN2012 database, J. Quant. Spectrosc. Radiative Transfer,130, 201–219, (2013).

Buchholz, B., Böse, N., and Ebert, V.: Absolute validation of a diode laser hygrometer via intercomparison with the German national primary water vapor standard, Appl. Phys. B., DOI: 10.1007/s00340-014-5775-4, 2014.

Buchholz, B., and Ebert, V.: Absolute, pressure-dependent validation of a calibration-free, airborne laser hygrometer transfer standard (SEALDH-II) from 5 to 1200 ppmv using a metrological humidity generator, Atmos. Meas. Tech., 11(1), 459-471, doi::10.5194/amt-11-459-2018, 2018.

Burkhardt, U., Kärcher, B.: Global radiative forcing from contrail cirrus, Nature Clim. Change, 1, 54–58, https://doi.org/10.1038/nclimate1068, 2011.

Danilin, M. Y., Popp, P. J., Herman, R. L., Ko, M. K. W., Ross, M. N., Kolb, C. E., Fahey, D. W., Avallone, L. M., Toohey, D. W., Ridley, B. A., Schmid, O., Wilson, J. C., Baumgardner, D. G., Friedl, R. R., Thompson, T. L., and Reeves, J. M.: Quantifying Uptake of HNO_3 and H_2O by Alumina Particles in Athena-II Rocket Plume, J. Geophys. Res., 108(D4), doi:10.1029/2002JD002601, 2003.

Davis, S. M., Avallone, L. M., Weinstock, E. M., Twohy, C. H., Smith, J. B., Kok, G. L.: Comparisons of in situ measurements of cirrus cloud ice water content, J. Geophys. Res.-Atmos., 112(D10), D10212, DOI: 10.1029/2006JD008214, 2007.

Diskin, G. S., Podolske, J. R., Sachse, G. W., and Slate, T. A.: Open-Path Airborne Tunable Diode Laser Hygrometer, Proc. SPIE, 4817, 196-204, 2002.

Drela, M.: http://web.mit.edu/drela/Public/web/xfoil/.

Ebert, V., Teichert, H., Giesemann, C., Saathoff, H., and Schurath, U.: Fibre-coupled in-situ laser absorption spectrometer for the selective detection of water vapour traces down to the ppb-level, Technisches Messen, 72, 23-30, 2005.

Engblom, W. A., and Ross, M. N.: Numerical Model of Airflow Induced Particle Enhancement for Instruments Carried by the WB-57F Aircraft, Aerospace Report No. ATR-2004(5084)-1, 2003.

Fahey, D. W., Gao, R.-S., Möhler, O., Saathoff, H., Schiller, C., Ebert, V., Krämer, M., Peter, T., Amarouche, N., Avallone, L. M., Bauer, R., Bozóki, Z., Christensen, L. E., Davis, S. M., Durry, G., Dyroff, C., Herman, R. L., Hunsmann, S., Khaykin, S., Mackrodt, P., Meyer, J., Smith, J. B., Spelten, N., Troy, R. F., Vömel, H., Wagner, S., and Weinhold, F. G.: The AquaVIT-1 Intercomparison of Atmospheric Water Vapor Measurement Techniques, Atmos. Meas. Tech. Disc., 7:3159-3251, 2014.

Froyd, K. D., Murphy, D. M., Lawson, P., Baumgardner, D., and Herman, R. L.: Aerosols that form subvisible cirrus at the tropical tropopause, Atmos. Chem. Phys., 10, 209-18, 2010.

Gao, R.-S., Popp, P. J., Fahey, D. W., Marcy, T. P., Herman, R. L., Weinstock, E. M., Baumgardner, D. G., Garrett, T. J., Rosenlof, K. H., Thompson, T. L., Bui, T. P., Ridley, B. A., Wofsy, S. C., Toon, O. B., Tolbert, M. A., Kaercher, B., Peter, T., Hudson, P. K., Weinheimer, A. J., and Heymsfield, A. J.: Evidence That Nitric Acid Increases Relative Humidity in Low-Temperature Cirrus Clouds, Science, 303, 516-20, 2004.

Gao, R. S., Fahey, D. W., Popp, P. J., Marcy, T. P., Herman, R. L., Weinstock, E. M., Smith, J. B., Sayres, D. S., Pittman, J. V., Rosenlof, K. H., Thompson, T. L., Bui, P. T., Baumgardner, D. G., Anderson, B. E., Kok, G., and Weinheimer, A. J.: Measurements of relative humidity in a persistent contrail, Atmos. Env., 40, 1590-1600, 2006.

https://doi.org/10.5194/egusphere-2024-4019
Preprint. Discussion started: 10 January 2025

Garrett, T. J., Navarro, B. C., Twohy, C. H., Jensen, E. J., Baumgardner, D. G., Bui, P. T., Gerber, H., Herman, R. L., Heymsfield, A. J., Lawson, P., Minnis, P., Nguyen, L., Poellot, M., Pope, S. K., Valero, F. P. J., and Weinstock, E. M.: Evolution of a Florida cirrus anvil, J. Atmos. Res., 62, 2353-72, 2005.

Gates, A. M., Avallone, L. M., Toohey, D. W., Rutter, A. P., Whitefield, P. D., Hagan, D. E., Hopkins, A. R., Ross, M. N., Zittel, P. F., Thompson, T. L., Herman, R. L., and Friedl, R. R.: In situ Measurements of Carbon Dioxide, 0.37-4.0 µm Particles, and Water Vapor in the Stratospheric Plumes of Small Rockets, J. Geophys. Res., 107(D22), doi:10.1029/2002JD002121, 2002.

Gensch, I. V., Bunz, H., Baumgardner, D. G., Christensen, L. E., Fahey, D. W., Herman, R. L., Popp, P. J., Smith, J. B., Troy, R. F., Webster, C. R., Weinstock, E. M., Wilson, J. C., Peter, T., and Krämer, M.: Supersaturations, microphysics and nitric acid partitioning in a cold cirrus observed during CR-AVE 2006: An observation-modeling intercomparison study, Environ. Res. Lett., 3, 035003, doi: 10.1088/1748-9326/3/3/035003, 2008.

Gettelman, A., Fetzer, E. J., Eldering, A., and Irion, F. W.: The global distribution of supersaturation in the upper troposphere from the Atmospheric Infrared Sounder. Journal of Climate, 19(23), 6089-6103, 2006.

Gordon, I. E., et al.: The HITRAN2020 molecular spectroscopic database, J. Quantitative Spectroscopy Radiative Transfer, 277, doi:10.1016/j.jqsrt.2021.107949, 2022.

Hallar, A. G., Avallone, L. M., Herman, R. L., Anderson, B. E., and Heymsfield, A. J.: Measurements of ice water content in tropopause region Arctic cirrus during the SAGE III Ozone Loss and Validation Experiment (SOLVE), J. Geophys. Res., 109, D17203, doi: 10.1029/2003JD004348, 2003.

Herman, R. L., Drdla, K., Spackman, J. R., Hurst, D. F., Popp, P. J., Webster, C. R., Romashkin, P. A., Elkins, J. W., Weinstock, E. M., Gandrud, B. W., Toon, G. C., Schoeberl, M. R., Jost, H.-J., Atlas, E. L., and Bui, T. P., Hydration, dehydration, and the total hydrogen budget of the 1999-2000 winter Arctic stratosphere, J. Geophys. Res., 108(D5), doi:10.1029/2001JD001257, 2003.

Herriott, D., Kogelnik, H., and Kompfner, R.: Off-Axis Paths in Spherical Mirror Interferometers, Appl. Optics, 3, 523-6, 1964.

Heymsfield, A. J., Miloshevich, L. M., Twohy, C., Sachse, G., and Oltmans, S.: Upper-tropospheric relative humidity observations and implications for cirrus ice nucleation. Geophysical Research Letters, 25(9), 1343-1346: 1998.

Hintsa, E. J., Weinstock, E. M., Anderson, J. G., and May, R. D.: On the accuracy of in situ water vapor measurements in the troposphere and lower stratosphere with the Harvard Lyman-alpha Hygrometer, J. Geophys. Res., 104(D7), 8183-9, 1999.

Hintsa, E., et al.: First Results from UCATS during the GloPac 2010 Mission, American Geophysical Union, Fall Meeting 2010, abstract #A51B-0093.

Humlicek, J.: Optimized computation of the Voigt and complex probability functions, J. Quant. Spectrosc. Radiat. Transfer, 27, 437, 1982.

Hurst, D. F., Dutton, G. S., Romashkin, P. A., Wamsley, P. R., Moore, F. L., Elkins, J. W., Hintsa, E. J., Weinstock, E. M., Herman, R. L., Moyer, E. J., Scott, D. C., May, R. D., and Webster, C. R.: Closure of the total hydrogen budget of the northern extratropical lower stratosphere, J. Geophys. Res., 104(D7), 8191-200, 1999.

Jensen, E. J., Smith, J. B., Pfister, L., Pittman, J. V., Weinstock, E. M., Sayres, D. S., Herman, R. L., Troy, R. F., Rosenlof, K., Thompson, T. L., Fridlind, A. M., Hudson, P. K., Cziczo, D. J., Heymsfield, A. J., Schmitt, C. and Wilson, J. C.: Ice Supersaturations Exceeding 100% at the Cold Tropical Tropopause: Implications for Cirrus Formation and Dehydration, Atmos. Chem. Phys., 5, 851-62, 2005.

Kirk-Davidoff, D. B., Hintsa, E. J., Anderson, J. G., and Keith, D. W.: The effect of climate change on ozone depletion through changes in stratospheric water vapour, Nature, 402, 399-401, doi:10.1038/46521, 1999.

https://doi.org/10.5194/egusphere-2024-4019
Preprint. Discussion started: 10 January 2025

Kley, D., Russell, J. M., III, and Phillips, C. (Eds.): SPARC Assessment of Upper Tropospheric and Stratospheric Water Vapour, World Meteorol. Org., Geneva, 2000.

Lee, D. S., Fahey, D. W., Skowron, A., Allen, M. R., Burkhardt, U., Chen, Q., Doherty, S. J., Freeman, S., Forster, P. M., Fuglestvedt, J., Gettelman, A., De León, R. R., Lim, L. L., Lund, M. T., Millar, R. J., Owen, B., Penner, J. E., Pitari, G., Prather, M. J., Sausen, R., and Wilcox, L. J.: The contribution of global aviation to anthropogenic climate forcing for 2000 to 2018, Atmos. Env., 244, 117834, https://doi.org/10.1016/j.atmosenv.2020.117834, 2021.

Lee, S.-H., Wilson, J. C., Baumgardner, D., Herman, R. L., Weinstock, E. M., LaFleur, B. G., Kok, G., Anderson, B., Lawson, P., Baker, B., Strawa, A., Pittman, J. V., Reeves, J. M., and Bui, T. P.: New particle formation observed in the tropical/subtropical cirrus clouds, J. Geophys. Res., 109, D20209, doi: 10.1029/2004JD005033, 2004.

May, R. D.: Open-path, near-infrared tunable diode laser spectrometer for atmospheric measurements of H_2O, J. Geophys. Res., 103(D15), 19161-19172, doi:10.1029/98jd01678, 1998.

May, R. D. and Webster, C. R.: Data processing and calibration for tunable diode laser harmonic absorption spectrometers, J. Quant. Spectrosc. Radiat. Transfer, 49, 335-47, 1993.

Peter, T., Marcolli, C., Spichtinger, P., Corti, T., Baker, M. B., and Koop, T.: When Dry Air Is Too Humid, Science, 314(5804), 1399-1402, 2006.

Podolske, J. R., Sachse, G. W., and Diskin, G. S.: Calibration and data retrieval algorithms for the NASA Langley/Ames Diode Laser Hygrometer for the NASA Transport and Chemical Evolution Over the Pacific (TRACE-P) mission, J. Geophys. Res., 108(D20), 8792, doi: 10.1029/2002jd003156, 2003.

Ray, E. A., Rosenlof, K. H., Richard, E. C., Hudson, P. K., Cziczo, D. J., Loewenstein, M., Jost, H.-J., Lopez, J., Ridley, B., Weinheimer, A., Montzka, D., Knapp, D., Wofsy, S. C., Daube, B. C., Gerbig, C., Xueref, I., and Herman, R. L.: Evidence of the effect of summertime midlatitude convection on the subtropical lower stratosphere from CRYSTAL-FACE tracer measurements, J. Geophys. Res., 109(D18), D18304, doi: 10.1029/2004JD004655, 2004.

Read, W. G., et al.: Aura Microwave Limb Sounder upper tropospheric and lower stratospheric H_2O and relative humidity with respect to ice validation, J. Geophys. Res. Atmospheres, 112(D24), D24S35, doi:10.1029/2007jd008752, 2007.

Richard, E. C., Tuck, A. F., Aikin, K. C., Kelly, K. K., Herman, R. L., Troy, R. F., Hovde, S. J., Rosenlof, K. H., Thompson, T. L., Murphy, D. M., and Ray, E. A.: High Resolution Airborne Profiles of CH_4, O_3 and Water Vapor near Tropical Central America in Late January - Early February 2004, J. Geophys. Res., 111, D13304, doi:10.1029/2005JD006513, 2006.

Ridley, B., Atlas, E., Selkirk, H., Pfister, L., Montzka, D., Walega, J., Donnelly, S., Stroud, V., Richard, E., Kelly, K., Tuck, A., Thompson, T., Reeves, J., Baumgardner, D., Rawlins, W. T., Mahoney, M., Herman, R., Friedl, R., Moore, F., Ray, E., and Elkins, J.: Convective transport of reactive constituents to the tropical and mid-latitude tropopause region: I. Observations, Atmos. Environ. 38(9), 1259-74, 2004.

Rodgers, C. D. and Connor, B. J.: Intercomparison of remote sounding instruments, J. Geophys. Res., 108, 4116, doi:10.1029/2002JD002299, 2003.

Rohart F., Colmont, J.-M., Wlodarczak, G., Bouanich J.-P.: N_2- and O_2-broadening coefficients and profiles for millimeter lines of $^{14}N_2O$, J. Mol. Spectros., 222(2), 159–71, 2003.

Rollins, A. W., Thornberry, T. D., Gao, R. S., Smith, J. B., Sayres, D. S., Sargent, M. R., Schiller, C., Krämer, M., Spelten, N., Hurst, D. F., Jordan, A. F., Hall, E. G., Vömel, H., Diskin, G. S., Podolske, J. R., Christensen, L. E., Rosenlof, K. H., Jensen, E. J., and Fahey, D. W.: Evaluation of UT/LS hygrometer accuracy by intercomparison during the NASA MACPEX mission, J. Geophys. Res., DOI: 10.1002/2013JD020817, 2014.

https://doi.org/10.5194/egusphere-2024-4019
Preprint. Discussion started: 10 January 2025

Rothman, L. S., et al.: The HITRAN2012 molecular spectroscopic database, J. Quant. Spectros. Rad. Trans., 130, 4-50, doi: http://dx.doi.org/10.1016/j.jqsrt.2013.07.002, 2013.

Sargent, M. R., Sayres, D. S., Smith, J. B., Witinski, M., Allen, N. T., Demusz, J. N., Rivero, M., Tuozzolo, C., and Anderson, J. G.: A new direct absorption tunable diode laser spectrometer for high precision measurement of water vapor in the upper troposphere and lower stratosphere, Rev. Sci. Instrum., 84, 074102, doi:http://dx.doi.org/10.1063/1.4815828, 2013.

Schneider, M., Hase, F., Blavier, J.-F., Toon, G. C., and Leblanc, T.: An empirical study on the importance of a speed-dependent Voigt line shape model for tropospheric water vapor profile remote sensing, J. Quant. Spectros. Rad. Trans., 112(3), 465–474, 2011.

Schwartz, M. J., Read, W. G., Santee, M. L., Livesey, N. J., Froidevaux, L., Lambert, A., and Manney, G. L.: Convectively injected water vapor in the North American summer lowermost stratosphere, Geophys. Res. Lett., 40, 2316-2321, doi:10.1002/grl.50421, 2013.

Skrotzki, J., Habig, J. C., and Ebert, V.; Integrative fitting of absorption line profiles with high accuracy, robustness, and speed, Appl. Phys. B, DOI 10.1007/s00340-013-5706-9, 2013.

Solomon, S., Rosenlof, K. H., Portmann, R. W., Daniel, J. S., Davis, S. M., Sanford, T. J., and Plattner, G.-K.: Contributions of Stratospheric Water Vapor to Decadal Changes in the Rate of Global Warming, Science, 327(5970), 1219-1223, doi:10.1126/science.1182488, 2010.

Sorenson, C. E., Forgione, J. B., Barnes, C. M., Van Gilst, D., and Sullivan, D.: The NASA Airborne Science Data and Telemetry System (NSADAT), Abstract IN11B-1283 presented at 2011 Fall Meeting, AGU, San Francisco, Calif., 5-9 Dec., 2011.

Troy, R. F.: Field Studies of ice supersaturations in the tropical tropopause layer, Ph.D. Dissertation, 177 pp., University of California at Los Angeles, Los Angeles, California, USA, 2007.

Voemel, H., David, D. E., and Smith, K.: Accuracy of tropospheric and stratospheric water vapor measurements by the cryogenic frost point hygrometer: Instrumental details and observations, J. Geophys. Res., 112, D08305, doi:10.1029/2006JD007224, 2007.

Webster, C. R., Menzies, R. T., and Hinkley, E. D.: Infrared laser absorption: theory and applications, Chapter 3 in Laser Remote Chemical Analysis, R.M. Measures, ed., Wiley, New York, 163-272, 1988.

Yoder, P. R.: Mounting Optics in Optical Instruments, 2nd ed., Society of Photo-Optical Instrumentation Engineers, Bellingham, Washington, 2008.

Zondlo, M. A., Paige, M. E., Massick, S. M., and Silver, J. A.: J. Geophys. Res., 115, D20309, doi:10.1029/2010JD014445, 2010.

https://doi.org/10.5194/egusphere-2024-4019
Preprint. Discussion started: 10 January 2025

TABLES

Table 1: History of JLH aircraft flights in NASA UT/LS field missions. The field mission acronyms are defined in footnotes below.

Mission*	Timeframe	JLH Mark1 (a)	JLH Mark1 (b) 2nd Build	JLH Mark2	Quality	Aircraft	Number of Flights	Air Base
NASA POLARIS	Spring-Summer 1997	✓			Good	ER-2	21	Fairbanks, Alaska
WAM	April, May 1998		✓		Good	WB-057	3	Houston, Texas
NASA ACCENT	1999		✓		Good	WB-57	8	Houston, Texas
NASA SOLVE	Jan-March 2000	✓	✓		Good	ER-2	17	Kiruna, Sweden
NASA CRYSTAL-FACE	2000		✓		Good	WB-57	13	Key West, Florida
NASA Pre-AVE	Jan-Feb 2004		✓		Lower S/N	WB-57	7	Alajuela, Costa Rica
NASA MidCix	Apr-May 2004		✓		Lower S/N	WB-57	7	Houston, Texas
PUMA	May 2004, Julu 2005		✓		Lower S/N	WB-57	9	Houston, Texas
NASA AVE	Oct-Nov 2004, Jun-Jul 2005		✓		Lower S/N	WB-57	18	Houston, Texas
NASA WIIM	Jul 2005		✓		Lower S/N	WB-57	4	Houston, Texas
NASA CR-AVE	Jan-Feb 2006		✓		Lower S/N	WB-57	16	Alajuela, Costa Rica
NASA TC4-Costa Rica	Aug 2007		✓		Very Good	WB-57	7	Alajuela, Costa Rica
AquaVIT-1	Oct 2007		✓		Very Good	AIDA	5	Karlsruhe, Germany
NASA NOVICE	Sep 2008		✓		Good	WB-57	3	Houston, Texas
NASA MACPEX	April 2011		✓		UT only, No LS	WB-57	5	Houston, Texas
NASA SEAC^{4}RS	Aug, Sep 2013			✓	Best	ER-2	21	Houston, Texas
NGC FTB	2015-2023			✓	Best	NGC G-II	109	Lancaster, California

*Definitions of acronyms follow (For the WB-57 aircraft missions see the url
http://jsc-aircraft-ops.jsc.nasa.gov/wb57/missions.html).

POLARIS: “Photochemistry of Ozone Loss in the Arctic Region In Summer”, https://cloud1.arc.nasa.gov/polaris/

WAM: “WB-57 Aerosol Mission” (see NASA JSC url above);

ACCENT: “Atmospheric Chemistry of Combustion Emissions Near the Tropopause” (see NASA JSC url above);

SOLVE: “SAGE III Ozone Loss and Validation Experiment”,
https://espo.nasa.gov/solve

CRYSTAL-FACE: “Cirrus Regional Study of Tropical Anvils and Cirrus Layers – Florida Area Cirrus Experiment”,
https://espo.nasa.gov/crystalface

https://doi.org/10.5194/egusphere-2024-4019
Preprint. Discussion started: 10 January 2025

Pre-AVE: “Pre Aura Validation Experiment”,
AVE: “Aura Validation Experiment” [includes AVE-Houston and maybe AVE-Houston2?]
WIIM: “Water Isotope Intercomparison Mission”;
CR-AVE: “Costa Rica – Aura Validation Experiment”,
https://espo.nasa.gov/ave-costarica2
TC4: “Tropical Composition, Cloud and Climate Coupling”,
https://espo.nasa.gov/tc4
AquaVIT-1 (not an acronym): “International Intercomparison of atmospheric Water Vapour Instruments”,
https://aquavit.icg.kfa-juelich.de/AquaVit/
NOVICE: “Newly-Operating and Validated Instruments Comparison Experiment”,
https://espo.nasa.gov/novice/
MACPEX: “Mid-latitude Airborne Cirrus Properties Experiment”,
https://espo.nasa.gov/macpex
SEAC^{4}RS: “Studies of Emissions and Atmospheric Composition, Clouds and Climate Coupling by Regional Surveys”,
https://espo.nasa.gov/missions/seac4rs

https://doi.org/10.5194/egusphere-2024-4019
Preprint. Discussion started: 10 January 2025

Table 2: Spectroscopic parameters from HITRAN for the water absorption line at 7299.4311 cm-1 sampled in this work (Rothman et al., 2013, and Gordon et al., 2022). HITRAN 2012 parameters were utilized in data processing in 2012-2023. The latest line parameters from HITRAN 2022 are shown in the right column for comparison.

Parameter	Name (units)	HITRAN 2012	HITRAN 2022
S	Intensity (cm^{-1}/(molecule cm^{-2}) at 296K)	1.005×10^{-20}	1.025×10^{-20}
E″	Lower-state energy (cm^{-1})	42.3717	42.3717
γ_{air}	Air-broadened half width at 296K (cm^{-1} atm^{-1})	0.1032	0.1069
γ_{self}	Self-broadened half width at 296K (cm^{-1} atm^{-1})	0.46	0.48
n	Temperature-dependent exponent for γ_{air}	0.69	0.76
δ	Air-pressure induced line shift (cm^{-1} atm^{-1} at 296K)	-0.00878	-0.0